Solution to the problem of the poor cyclic fatigue resistance of bulk metallic glasses

Maximilien E. Launey[a], Douglas C. Hofmann[b], William L. Johnson[b,1], and Robert O. Ritchie[a,c,1]

[a]Materials Sciences Division, Lawrence Berkeley National Laboratory, Berkeley, CA 94720; [b]Keck Laboratory of Engineering Materials, California Institute of Technology, Pasadena, CA 91125; and [c]Department of Materials Science and Engineering, University of California, Berkeley, CA 94720

Contributed by William L. Johnson, January 22, 2009 (sent for review December 12, 2008)

The recent development of metallic glass-matrix composites represents a particular milestone in engineering materials for structural applications owing to their remarkable combination of strength and toughness. However, metallic glasses are highly susceptible to cyclic fatigue damage, and previous attempts to solve this problem have been largely disappointing. Here, we propose and demonstrate a microstructural design strategy to overcome this limitation by matching the microstructural length scales (of the second phase) to mechanical crack-length scales. Specifically, semisolid processing is used to optimize the volume fraction, morphology, and size of second-phase dendrites to confine any initial deformation (shear banding) to the glassy regions separating dendrite arms having length scales of ≈2 μm, i.e., to less than the critical crack size for failure. Confinement of the damage to such interdendritic regions results in enhancement of fatigue lifetimes and increases the fatigue limit by an order of magnitude, making these ''designed'' composites as resistant to fatigue damage as high-strength steels and aluminum alloys. These design strategies can be universally applied to any other metallic glass systems.

composites | damage confinement | endurance limit | semisolid processing

Monolithic bulk metallic glasses (BMGs) have emerged over the past 15 years as a class of materials with unique and unusual properties that make them potential candidates for many structural applications (1). These properties include their near theoretical strengths combined with high formability, low damping, large elastic strain limits, and the ability to be thermoplastically formed into precision net shape parts in complex geometries (2, 3), all of which are generally distinct from, or superior to, corresponding crystalline metals and alloys. However, monolithic BMGs can also display less desirable properties that have severely restricted their structural use. In particular, properties limited by the extension of cracks, such as ductility, toughness, and fatigue, can be compromised in BMGs by inhomogeneous plastic deformation at ambient temperatures where plastic flow is confined in highly localized shear bands (4, 5). Such severe strain localization with the propagation of the shear bands is especially problematic under tensile stress states where catastrophic failure can ensue along a single shear plane with essentially zero macroscopic ductility (6, 7). Consequently, resulting plane-strain K_{Ic} fracture toughnesses in monolithic BMGs are often low (≈15–20 MPa$\sqrt{m}$), as compared with most crystalline metallic materials, although they are an order of magnitude larger than those for (ceramic) oxide glasses (8, 9). If such strain localization is suppressed such that plastic flow is allowed to be extensive, for example, by blunting the crack tip, then damage would be distributed over larger dimensions with toughness values increasing to ≈50 MPa$\sqrt{m}$ or more (8, 10). Whereas some metallic glasses appear to be intrinsically brittle in their as-cast state (11), others become severely embrittled on annealing due to structural relaxation and associated loss of free volume, elastic stiffening, or increasing yield strength, all leading to a reduction in the fracture toughness to values as low as those of ceramic glasses (11–15).

In addition to having questionable tensile ductility and toughness, monolithic BMGs are particularly susceptible to damage caused by cyclic loading. Although the macroscale crack propagation rate behavior is generally comparable to that for crystalline metals and alloys (10, 16), the fatigue resistance in terms of the 10^7-cycle endurance strength (or fatigue limit) tends to be particularly low for metallic glasses in both bulk and ribbon form (17–22). Measurements on Zr-based glasses, for example, reveal a fatigue limit* in four-point bending of ≈1/10 of the (ultimate) tensile strength or lower (20–22), in contrast with most crystalline metallic materials where fatigue limits are typically between 1/2 and 1/3 of their tensile strengths. Given the high strength (≈1 GPa or more) of many metallic glasses and their known resistance to the initiation of plastic flow under monotonic loading, these observations of very low fatigue limits are both surprising and disappointing.

We reason that the low fatigue limits result simply from the lack of microstructure in monolithic BMGs; the incorporation of a second phase in monolithic BMGs would therefore provide a potential solution. Indeed, with the recent development of in situ BMG-matrix composites, the problems of poor ductility and toughness in BMGs have been mitigated by the presence of such a second phase that provides a means to arrest the propagation of shear bands (23–26). However, to date, attempts to similarly enhance the corresponding fatigue resistance have been largely unsuccessful (27–29). In fact, one study (29) found that the fatigue life was actually reduced, compared with the monolithic glass, after incorporation of a second dendritic phase. We believe that the disappointing results obtained so far are because inadequate attention has been paid to the dimensions of the incorporated microstructure. Accordingly, we demonstrate here that, by introducing a second phase in the form of crystalline dendrites and by creating an effective interaction between the length scales of the shear bands and that of the dendrites, the fatigue limit can be raised significantly, by as much as an order of magnitude, to approach values comparable to that of high-strength crystalline metallic materials.

Results

Here, we examine a $Zr_{39.6}Ti_{33.9}Nb_{7.6}Cu_{6.4}Be_{12.5}$ BMG-matrix composite that was developed for high toughness (26); this alloy, termed DH3, comprises crystalline (β-phase) dendrites within an amorphous matrix. In earlier versions of such composite alloys, cooling rate variations within the ingots caused large differences in the overall dendrite length scale, with interdendrite spacings varying by 2 orders of magnitude (from ≈1 to 100

Author contributions: M.E.L., D.C.H., W.L.J., and R.O.R. designed research; M.E.L. and D.C.H. performed research; M.E.L., D.C.H, W.L.J., and R.O.R. analyzed data; and M.E.L., D.C.H., W.L.J., and R.O.R. wrote the paper.

The authors declare no conflict of interest.

[1]To whom correspondence may be addressed. E-mail: wlj@caltech.edu or roritchie@lbl.gov.

*The fatigue limit is expressed here in the usual way in terms of the applied stress amplitude, σ_a, which is defined as $\frac{1}{2}(\sigma_{max} - \sigma_{min})$, where σ_{max} and σ_{min} are, respectively, the maximum and minimum applied stresses in the loading cycle. The alternating stress is one-half of the stress range, $\Delta\sigma$.

 www.pnas.org/cgi/doi/10.1073/pnas.0900740106

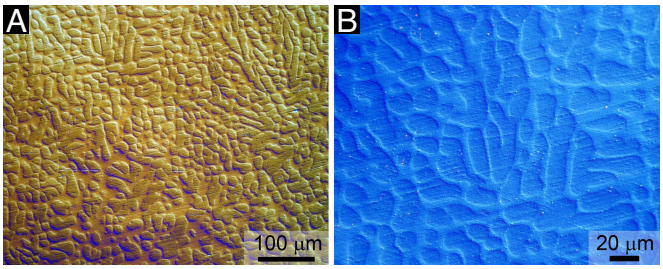

Fig. 1. Microstructure of the $Zr_{39.6}Ti_{33.9}Nb_{7.6}Cu_{6.4}Be_{12.5}$ (DH3) amorphous alloy. Z-contrast optical micrographs of the cross-section (*A*) and tensile surface (*B*) of a beam show a uniform two-phase microstructure throughout the ingot that comprises 67% dendritic phase by volume in a glass matrix. The dendritic phase is a ductile body-centered cubic solid solution containing primarily Zr, Ti, and Nb. Semisolid processing allows optimization of the volume fraction, morphology, and size of dendrites. This process leads to a homogeneous dispersion of a second phase separated by ≈2 μm of glass and guarantees an effective interaction between the dendrites and the shear bands.

μm) (23, 30). Consequently, to achieve control over the volume fraction, morphology, and size of the dendrites, we semisolidly processed (26) our material by heating into the semisolid two-phase region between the liquidus and solidus temperature, holding it isothermally for several minutes, and then quenching to vitrify the remaining liquid. This process yields a uniform two-phase microstructure throughout the ingot (Fig. 1), consisting of 67 vol % of the dendritic phase, a ductile (body-centered cubic) β-phase solid solution containing primarily Zr, Ti, and Nb, within a glass matrix (26). The compositions are $Ti_{45}Zr_{40}Nb_{14}Cu_1$ for the dendrites and $Zr_{34}Ti_{17}Nb_2Cu_9Be_{38}$ for the glass matrix. By tailoring the characteristic thickness of the glassy regions, which separate the dendrite arms or neighboring dendrites, to be smaller than the critical crack size that leads to unstable crack propagation, we have achieved alloys displaying 1.2–1.5 GPa yield strengths with tensile ductilities exceeding 10%.

With respect to fatigue resistance, we reason that, by similarly limiting the interdendrite spacing to provide "microstructural arrest barriers," we could curtail the extension of any incipient fatigue cracks to a length that would not cause catastrophic failure and thereby raise the fatigue limit. To investigate this hypothesis, we performed stress–life (*S–N*) fatigue testing to measure *S–N* (Wöhler) curves for the DH3 in situ BMG-matrix composite material and compared the data with results for other amorphous and crystalline metallic alloys. Our results are shown in Fig. 2 in the form of Wöhler plots of the number of loading cycles to failure, N_f, as a function of the applied stress amplitude, σ_a (= $(\sigma_{max} - \sigma_{min})/2$), normalized by the tensile strength, σ_{UTS}, at a stress ratio R (= $\sigma_{min}/\sigma_{max}$) of 0.1. We find that the normalized fatigue limit of our DH3 composite, defined as the $R = 0.1$ endurance strength at 2×10^7 cycles, is $\sigma_a/\sigma_{UTS} \approx 0.3$, i.e., $\sigma_a \approx 0.34$ GPa. This is substantially higher than that for monolithic BMGs; the commonly used Vitreloy 1 ($Zr_{41.25}Ti_{13.75}Ni_{10}Cu_{12.5}Be_{22.5}$) alloy displays a factor of nearly 10 times lower normalized fatigue limit of only $\sigma_a/\sigma_{UTS} \approx 0.04$, i.e., $\sigma_a = 0.075$ GPa (20, 21), and the older monolithic ribbon metallic glasses have fatigue limits that can drop as low as $\sigma_a/\sigma_{UTS} \approx 0.05$ (17–19). The fatigue limit of the DH3 composite is also 3 times higher than results for other in situ composite metallic glasses containing ductile dendrites; two alloys to date have been evaluated in fatigue, the $Zr_{56.2}Ti_{13.8}Nb_{5.0}Cu_{6.9}Ni_{5.6}Be_{12.5}$ (LM2) and $Cu_{47.5}Zr_{38}Hf_{9.5}Al_5$ alloys, where the fatigue limits were measured as $\sigma_a/\sigma_{UTS} \approx 0.1$ (27–29). In fact, compared with monolithic metallic glasses, which display some of the lowest fatigue limits of any metallic

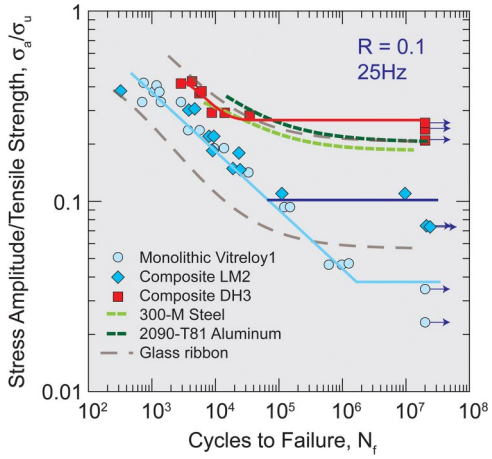

Fig. 2. Stress–life fatigue data (*S–N*). *S–N* curves are presented in terms of the number of cycles to failure, N_f, and stress amplitude (σ_a) normalized by the ultimate tensile strength of the material (σ_{UTS}). Both the fatigue lives and the fatigue limit (defined as an endurance strength, i.e., in terms of the alternating stress to yield lifetimes in excess of 2×10^7 cycles at a load ratio of 0.1) of the "designed composite" DH3 alloy are 1 order of magnitude higher than that of the monolithic bulk metallic glass (Vitreloy 1) (20, 21) that has a composition close to that of the matrix of our DH3 alloy. Indeed, the σ_a fatigue limit of DH3 is 28% of its ultimate tensile strength (σ_{UTS} = 1,210 MPa) (26), which is comparable with those of high-strength steel (300M) (31) and aluminum (2090-T81) (32) alloys. The confinement of shear bands under a critical length scale is a *sine qua non* condition to an effective increase of the fatigue limit. When the interdendritic spacing is too large, the dendrites do not effectively limit the initial propagation of small cracks, and little effect on the fatigue limit is detected. Previous attempts (28) to use glass-matrix composite microstructures, i.e., the $Zr_{56.2}Ti_{13.8}Nb_{5.0}Cu_{6.9}Ni_{5.6}Be_{12.5}$ (LM2) alloy, which was an in situ composite containing a dispersion of ≈10-μm-spaced dendritic second phase, gave fatigue limits that were only 10% of their tensile strengths. This was better than the worst-case monolithic BMG alloy (Vitreloy 1) (20, 21) but still poor compared with crystalline metals and alloys, because the spacing of the second phase was too coarse to be an effective barrier to the propagation of shear bands and the initial growth of small fatigue cracks. Fatigue data for monolithic metallic-glass ribbons, taken from refs. 17–19, are also plotted.

materials, the current DH3 glass-matrix composite has a normalized fatigue limit comparable with structural steels and aluminum alloys; specifically, it is >30% higher than that of a 300M ultra-high-strength steel (σ_{UTS} = 2.3 GPa) (31) and 2090-T81 aluminum–lithium alloys (σ_{UTS} = 0.56 GPa) (32), where at this stress ratio (R = 0.1) $\sigma_a/\sigma_{UTS} \approx 0.2$. The substantially higher fatigue limit in the current "designed" glass-matrix composite alloy, as compared with the monolithic glass alloy, translates of course into many orders of magnitude increase in the useful fatigue life of the material.

Discussion

The Model. The second-phase dendrites are the essential feature leading to the enhancement of the fatigue resistance of our composite BMG alloys to levels of $\sigma_a/\sigma_{UTS} \approx 0.3$ that are comparable to those of high-strength crystalline metallic materials. This approach of adding a second phase to enhance the fatigue limit has been used previously, and yet in these previous studies the normalized fatigue limit remained relatively low ($\sigma_a/\sigma_{UTS} \approx 0.1$) (27–29). However, as discussed below, it is the characteristic dimensions of this second phase compared with pertinent mechanical length scales that is the key to attaining good fatigue properties in metallic glass materials. Indeed, very recent studies on Ti- and Cu-based BMGs (33, 34) reinforced with nanocrystalline dispersions provide phenomenological evidence to support this notion, because the finer second-phase

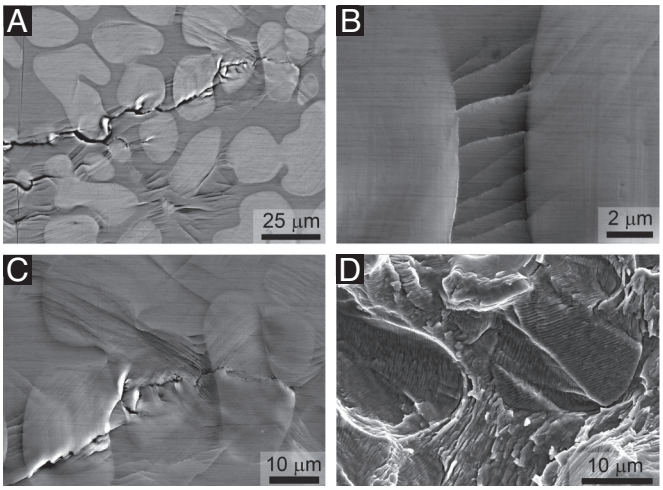

Fig. 3. Mechanisms of fatigue-crack initiation and propagation. (*A*) Scanning electron microscopy back-scattered image of a fatigue crack on the tensile surface showing a wide distribution of damage around the crack tip. Deformation occurs through the development of highly organized patterns of regularly spaced shear bands distributed uniformly along the crack path. (*B*) Secondary electron micrograph showing the interdendritic and shear-band spacing. Shear bands initiate and propagate inside the glass matrix until they are blocked by the dendrites. As the strain increases, shear bands multiply in several directions and interact with each other. Shear bands first move around the dendrites, but at higher stress levels they cut through the crystalline second phase. Microcracks are nucleated along the shear bands or at the matrix–dendrite interface (*A*). Crack propagation follows the shear-band propagation. (*C*) Secondary electron micrograph showing that the bands do not preferentially avoid the second-phase regions because they are observed to intersect the second phase closest to the crack path. (*D*) Secondary electron micrograph of the fracture surface showing apparent fatigue striations in both the crystalline and the amorphous phases. The crack-advance mechanism associated with irreversible crack-tip shear alternately blunts and resharpens the crack during each fatigue cycle. The fatigue crack in *A*, *C*, and *D* propagates from left to right.

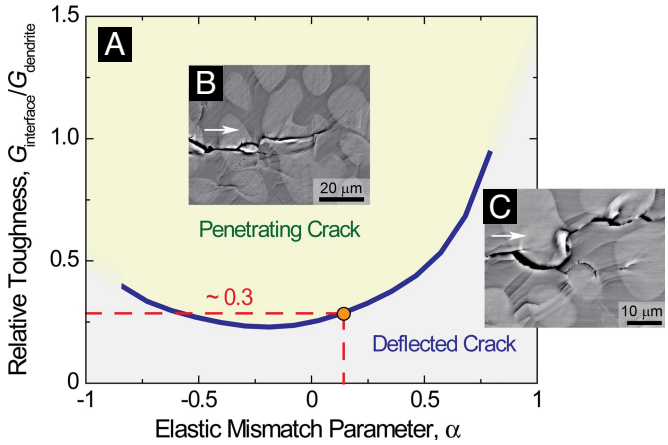

Fig. 4. The linear-elastic crack-deflection mechanics solution of He and Hutchinson (35) for a crack normally impinging an interface between two elastically dissimilar materials. (*A*) The curve marks the boundary between systems in which cracks are likely to penetrate the interface (above the curve) (*B*) or arrest or deflect along the interface (below the curve) (*C*). (*A*) Plot of the relative magnitude of the interface toughness and the toughness of the dendritic phase on the far side of the interface, $G_{interface}/G_{dendrite}$, as a function of the elastic mismatch defined by the first Dundurs' parameter (49), $\alpha = (E_{glass} - E_{dendrite})/(E_{glass} + E_{dendrite})$. For the glass–dendrite junction where $\alpha \approx 0.14$, the absence of interface delamination leads to a criticality between penetration and arrest or deflection at the interface, which can be used to estimate that the interface toughness must be <30% of the toughness of the dendrites for the latter phase to be effective in impeding the initial propagation of shear-band cracks. The arrows in *B* and *C* indicate the general direction of crack propagation.

distributions were also found to improve the fatigue strength by a factor of 2 to 3.

In the DH3 composite alloy, plastic deformation occurs uniformly throughout the material with the development of organized patterns of regularly spaced shear bands in the glassy regions between the arms of a single dendrite and regions separating neighboring dendrites. Fig. 3*A* and *C* shows typical shear-band patterns surrounding propagating microcracks (during fatigue). The path of the cracks (Fig. 3*A*) meanders alternately along matrix–dendrite interfaces, cutting through dendrite arms, and along existing shear bands in the glass separating the dendrite arms. Fig. 3*B* shows a typical set of shear bands confined between dendrite arms. The low shear modulus of the dendrite results in shear bands being attracted to the dendrites. Confinement is a result of the mismatch in plastic response. For instance, the dendrite deforms by dislocation slip and may undergo work hardening that stabilizes the shear band.

A primary issue for fatigue resistance is whether the second-phase dendrites can prevent single shear-band failure by arresting the initial shear-band cracks. Insight into this can be gleaned from the He and Hutchinson linear-elastic crack-deflection mechanics solution (35) that considers the situation of a crack impinging on a bimaterial interface and whether it will penetrate the dendrite or arrest or deflect there. This criticality depends specifically on the angle of crack incidence, the elastic mismatch across the interface, which is a function of the relative Young's moduli, i.e., the first Dundurs' parameter $\alpha = (E_{glass} - E_{dendrite})/(E_{glass} + E_{dendrite})$, and the ratio of fracture toughnesses of the interface and the material on the far side of the interface ($G_{interface}/G_{dendrite}$). This solution is plotted in Fig. 4 for the glass–dendrite interface with a normally incident crack and shows the regimes of relative interfacial toughness vs. relative elastic modulus where the crack will be arrested or deflected at the interface or penetrate it. Normal incidence along the boundary represents the geometrically worst-case scenario; a shallower angle increases the likelihood for crack deflection. Included are images of cracks in our alloy (DH3) at near 90° incidence. Using the values of elastic modulus, E, for both the glass and the dendritic phase (26), we can estimate that, for the dendrites to be an effective barrier to the propagation of a shear-band crack, the interfacial toughness must be <30% of the toughness of the dendritic phase.

Although it is uncertain exactly how a shear band evolves into a crack, it is clear that crack propagation between dendrite arms occurs along existing shear bands (Fig. 3 *A* and *B*). From a microscopic perspective, to propagate a microcrack between dendrite arms, a shear band must open by a cavitation mechanism. When a shear band slips, material in the core is energized by mechanical work that is converted to stored configurational enthalpy, heat, or both (36, 37). This softens the shear-band core, lowers the local shear modulus and the flow stress, and must also lower the barrier for cavitation induced by an opening stress. The extent of softening is a function of the total strain within the band (36) and thus the band width and the shear offset. In turn, the shear offset must scale with shear-band length. If the shear-band length is limited to the separation of dendrite arms (to several micrometers, as in Fig. 3*C*), then cavitation will be effectively suppressed. Higher stress levels are required to "open" the confined shear band compared with a much longer unconfined shear band. In turn, this elevates the applied stress levels for cavitation and propagation of the crack along the shear band. In steady-state fatigue-crack propagation, crack advance must be actually associated with an alternate blunting and resharpening mechanism as demonstrated by striations on the fracture surface

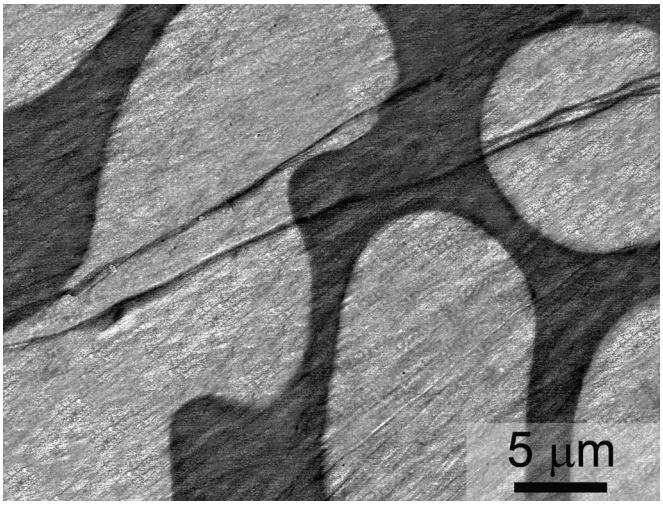

Fig. 5. Dormant shear bands: scanning electron microscopy back-scattered electron image of the cross-section of a beam tested at the fatigue limit after 2×10^7 cycles. Shear bands are observed near the tensile surface. Damage evolution occurs very early after only a few cycles. Some studies (16, 21) have suggested that the low fatigue limit reported for bulk metallic glasses may be associated with the presence of preexisting, micrometer-sized surface shear bands. In the current alloy, such shear bands are constrained by the crystalline second-phase dendrites to a length where they remain essentially dormant at the given stress amplitude, $\sigma_a/\sigma_{UTS} \approx 0.3$. The high fatigue limit of this material lies in its ability to provide microstructural barriers necessary to avoid propagation of the damage to critical size.

in both the dendrite and the glassy phases as seen in Fig. 3*D*. The cavitation during a stress cycle therefore must occur within an individual striation.

How does the above discussion relate to fatigue limits? For crystalline metals, fatigue lifetimes are largely dominated by the loading cycles required to initiate damage as opposed to propagating a "fatal" crack. The term initiation, however, is often a misnomer, because the rate-limiting process is generally not crack initiation but rather early propagation of small (often preexisting) flaws through a dominant microstructural barrier, e.g., a grain boundary or hard second-phase particle (38, 39). The lower fatigue limits of amorphous alloys can be attributed to the lack of a microstructure that provides local arrest points for newly initiated or preexisting cracks (16, 20, 21). Small cracks are observed to initiate after only a few stress cycles in BMGs (21). In contrast to crystalline alloys, fatigue lifetimes should therefore be governed by early crack propagation (rather than initiation), specifically by the number of cycles to extend a small flaw to some critical size (Fig. 5). In the present case of the BMG-matrix composite, the critical flaw size must be greater than some feature of the dendritic microstructure (i.e., the interarm spacing) to prevent unstable crack propagation.

To prevent a shear band from opening and causing failure between dendrite arms, the shear-band length must fall below a critical size that is determined by the applied stress and fracture toughness of the BMG. For high-cycle fatigue resistance, the dendrites must also limit microcrack growth (during 10^7 cycles) in the fatigue limit to a similar length. We illustrate this argument with a simple fracture-mechanics calculation. Considering the interdendritic shear bands (Fig. 3*A*) as small cracks modeled as edge cracks in bending, the approximate stress intensity (40) at the tip of a single interdendritic shear band of 2 μm in length would be 1.9 MPa$\sqrt{\text{m}}$ at the stress, corresponding to the fatigue limit of $\sigma_a = 0.3\sigma_{UTS}$. This is approximately equal to the measured fatigue-crack-growth threshold stress intensity for the monolithic glass (10, 16) and is consistent with no failure in the BMG composite at 2×10^7 cycles. In contrast, for the LM2 glass-matrix composite with a smaller volume fraction of dendrites and interdendritic glass thicknesses of $\approx$10 μm (23, 28), a shear band could grow 5 times larger before arrest by the dendrites. The threshold stress intensity can now be reached at much lower applied stress of $\sigma_a = (0.3/5^{1/2})\sigma_{UTS} \approx 0.1\sigma_{UTS}$, as observed experimentally. This presents a simple hypothesis for improving the low fatigue limits in metallic glasses. The characteristic spacing, D, which separates second-phase inclusions in a glassy matrix (and thereby confines the shear-band length), should be such that $\alpha\sigma_a D^{1/2} \sim K_{th}$, where K_{th} is the critical stress-intensity threshold for fatigue-crack propagation in the monolithic glass and α is a constant of order unity. Equivalently, one predicts a fatigue limit of $\sigma_a \sim K_{th}/\alpha D^{1/2}$. In the absence of any microstructure, as in monolithic BMG, it is clear that fatigue limits will be very low because D becomes essentially infinitely large.

Other Considerations. In addition to the spacing, one might ask whether the microstructural topology of the dendritic phase is also important. This is especially pertinent to in situ glass-matrix composites, because recent studies on La-based BMG–dendrite alloys have shown that the ductility and toughness of these alloys, at both room (41) and elevated (42) temperatures, can be quite different above and below the percolation threshold for the second-phase dendrites. Whereas this may be important for "global" properties such as the resistance to fatigue-crack propagation (and ductility and toughness) where a crack could span many characteristic microstructural dimensions, we doubt whether it would have too much influence on a property such as the fatigue limit, which depends on distinctly "local" phenomena, specifically the initiation and early growth of a micrometer-sized shear-band crack within the glassy phase and its arrest at the glass–dendrite interface.

One might also argue that the fatigue limits of the BMG-composite alloys are much higher than those of the monolithic BMG materials simply because they contain a high fraction of a crystalline (dendritic) phase. However, in similar vein, because the critical event associated with the definition of the fatigue limit is the local arrest of a small crack at the BMG–dendrite interface, the fatigue properties of the dendritic phase itself are far less important than the crack-arresting capability of the interface.

Finally, there are data in the literature, specifically from Liaw and co-workers (43–45), that report extremely high σ_a fatigue limits for several monolithic Zr-based BMG alloys that are as large as $\approx 0.25\sigma_{UTS}$, results that are totally inconsistent with fatigue-limit measurements by other investigators (20, 21) on similar alloys that we have quoted in this article. We believe that there are two reasons for this inconsistency. First, as suggested by Schuh et al. (46), the Liaw group's specimens were machined from relatively small ingots, whereas those used by other investigators (16, 20–22) were machined from cast plates. Although this could have led to differences in free volume and residual stresses due to variations in cooling (15, 47), we do not believe that this factor is that significant. A second, more significant reason is that there is a major difference in the specimen geometries used; Liaw and co-workers (43–45) used a notched cylinder geometry whereas all other investigators have used unnotched rectangular bend bars. For the measurement of material properties, such as fatigue limits, the notched geometry used by Liaw and co-workers is a particularly poor choice, simply because there will always be significant uncertainty in the value of the stress

concentration factor to use to define the fatigue-limit stress.[†] Indeed, after careful analysis of the stress state and final fracture surfaces for the notched specimens of Liaw and co-workers (43, 44), Menzel and Dauskardt (48) concluded that an incorrect stress concentration factor had been used. It is for this reason that we strongly believe that the unsubstantiated and unreasonably high fatigue limits measured by Liaw and his colleagues (43–45) are in error.

Closure. In conclusion, our results on the new DH3 alloy highlight the potential of using designed composite microstructures for bulk metallic glass alloys to provide an effective solution, not simply to their low tensile ductility and toughness but also to their characteristically poor stress–life fatigue properties. Provided the characteristic length scales of crack size and microstructure are correctly matched, both to retard the initial extension of small flaws and to prevent single shear-band opening failure, BMG materials can be made with high strength (>1.2 GPa), substantial tensile ductility (>10%), and fatigue limits that exceed those of high-strength steels and aluminum alloys.

Methods

Design of Alloys. The metallic glass-matrix $Zr_{39.6}Ti_{33.9}Nb_{7.6}Cu_{6.4}Be_{12.5}$ alloys used in this research were prepared in a two-step process. First, ultrasonically cleansed pure elements, with purities 99.5%, were arc-melted under a Ti-gettered argon atmosphere. The ingots were formed by making master ingots of Zr–Nb and then combining those ingots with Ti, Cu, and Be. Ti and Zr crystal bars were used, and other elements were purchased from Alfa Aesar in standard forms. Second, the ingots were placed on a water-cooled Cu boat and heated via induction, with temperature monitored by pyrometer. The second step was used as a way of semisolidly processing the alloys between their solidus and liquidus temperatures. This procedure coarsens the dendrites, produces radio-frequency stirring, and homogenizes the mixture. Samples were produced with masses up to 35 g and with thicknesses of 10 mm, based on the geometry of the Cu boat. Samples for mechanical testing were machined directly from these ingots.

Characterization. Microstructures were characterized using an interference contrast technique on a Axiotech 100 reflected-light microscope (Carl Zeiss MicroImaging) and scanning electron microscopy (SEM) (S-4300SE/N ESEM; Hitachi America) operating in vacuo (10^{-4} Pa) at a 30-kV excitation voltage in both secondary and back-scattered electron modes. Samples were mechanically wet polished with an increasingly higher finish to a final polish with a 1-μm diamond suspension. No etching was performed.

Stress–Life Experiments. Fatigue-life (*S–N*) curves were measured over a range of cyclic stresses by cycling $3 \times 3 \times 50$ mm rectangular beams in four-point bending (tension–tension loading) with an inner loading span, S_1, and outer span, S_2, of 15 and 30 mm, respectively, in a computer-controlled, servo-hydraulic MTS 810 mechanical testing machine (MTS Corporation). The corners of the beams were slightly rounded to reduce any stress concentration along the beam edges, and they were then polished with diamond paste to a 1-μm finish on the tensile surface before testing. Testing was conducted in room air under load control with a frequency of 25 Hz (sine wave) and a constant load ratio (ratio of minimum to maximum load, $R = P_{min}/P_{max}$) of 0.1. Stresses were calculated at the tensile surface within the inner span using the simple beam mechanics theory:

$$\sigma = \frac{3P(S_2 - S_1)}{2BW^2}, \qquad [1]$$

where P is the applied load, B is the specimen thickness, and W is the specimen height. Beams were tested at maximum stresses ranging from 560 to 1,150 MPa (just below the ultimate tensile strength). Tests were terminated in cases where failure had not occurred after 2×10^7 cycles (≈9 days at 25 Hz). Fracture surfaces of selected beams were examined after failure by both optical microscopy and SEM to discern the origin and mechanisms of failure. The stress–life fatigue data (*S–N*), shown in Fig. 2, are presented in terms of the number of cycles to failure, N_f, and stress amplitude ($\sigma_a = \frac{1}{2}\Delta\sigma = \frac{1}{2}[\sigma_{min} - \sigma_{max}]$) normalized by the ultimate tensile strength of the material (σ_{UTS}), where $\Delta\sigma$ is the stress range and σ_{max} and σ_{min} correspond, respectively, to the maximum and minimum values of the applied loading cycle.

ACKNOWLEDGMENTS. M.E.L. and R.O.R. acknowledge financial support from the Director, Office of Science, Office of Basic Energy Sciences, Division of Materials Sciences and Engineering, of the U.S. Department of Energy under Contract DE-AC02-05CH11231. D.C.H. acknowledges financial support from the Department of Defense through the National Defense Science and Engineering Graduate Fellowship program. D.C.H. and W.L.J acknowledge funding support through the Office of Naval Research.

[†]The stress concentration factor under fatigue conditions is invariably not the elastic stress concentration factor, k_t, which can be well defined by the geometry and loading conditions. In fatigue, an effective stress concentration factor, k_f, must be used that will be less than or equal to k_t, depending upon the material and size of the notch. Because the value of k_f cannot be predicted or even calculated, it must be defined from experimental data in terms of the ratio of the alternating stress to give a specific life in an unnotched fatigue test divided by the corresponding alternating stress to give the same life in a notched test, a procedure that was not utilized by Liaw and co-workers (43–45).

1. Byrne CJ, Eldrup M (2008) Materials science: Bulk metallic glasses. *Science* 321:502–503.
2. Ashby MF, Greer AL (2006) Metallic glasses as structural materials. *Scr Mater* 54:321–326.
3. Schroers J (2005) The superplastic forming of bulk metallic glasses. *JOM* 57:35–39.
4. Pampillo CA (1975) Flow and fracture in amorphous alloys. *J Mater Sci* 10:1194–1227.
5. Greer AL (1995) Metallic glasses. *Science* 267:1947–1953.
6. Bruck HA, Christman T, Rosakis AJ, Johnson WL (1994) Quasi-static constitutive behavior of $Zr_{41.25}Ti_{13.75}Ni_{10}Cu_{12.5}Be_{22.5}$ bulk amorphous-alloys. *Scr Metall Mater* 30:429–434.
7. Flores KM, Dauskardt RH (2001) Mean stress effects on flow localization and failure in a bulk metallic glass. *Acta Mater* 49:2527–2537.
8. Flores KM, Dauskardt RH (1999) Enhanced toughness due to stable crack tip damage zones in bulk metallic glass. *Scr Mater* 41:937–943.
9. Lowhaphandu P, Lewandowski JJ (1998) Fracture toughness and notched toughness of bulk amorphous alloy: Zr-Ti-Ni-Cu-Be. *Scr Mater* 38:1811–1817.
10. Gilbert CJ, Ritchie RO, Johnson WL (1997) Fracture toughness and fatigue-crack propagation in a Zr-Ti-Ni-Cu-Be bulk metallic glass. *Appl Phys Lett* 71:476–478.
11. Lewandowski JJ, Wang WH, Greer AL (2005) Intrinsic plasticity or brittleness of metallic glasses. *Philos Mag Lett* 85:77–87.
12. Lewandowski JJ (2001) Effects of annealing and changes in stress state on fracture toughness of bulk metallic glass. *Mater Trans* 42:633–637.
13. Suh D, Dauskardt RH (2003) Effects of open-volume regions on relaxation time-scales and fracture behavior of a Zr-Ti-Ni-Cu-Be bulk metallic glass. *J Non-Cryst Solids* 317:181–186.
14. Murah P, Ramamurty U (2005) Embrittlement of a bulk metallic glass due to sub-T_g annealing. *Acta Mater* 53:1467–1478.
15. Launey ME, Busch R, Kruzic JJ (2008) Effects of free volume changes and residual stresses on the fatigue and fracture behavior of a Zr-Ti-Ni-Cu-Be bulk metallic glass. *Acta Mater* 56:500–510.
16. Gilbert CJ, Schroeder V, Ritchie RO (1999) Mechanisms for fracture and fatigue-crack propagation in a bulk metallic glass. *Metall Mater Trans A* 30:1739–1753.
17. Ogura T, Masumoto T, Fukushima K (1975) Fatigue fracture of amorphous Pd-20at.%.Si alloy. *Scr Metall* 9:109–113.
18. Davis LA (1976) Fatigue of metallic glasses. *J Mater Sci* 11:711–717.
19. Alpas AT, Edwards L, Reid CN (1989) Fracture and fatigue crack-propagation in a nickel-base metallic glass. *Metall Mater Trans A* 20:1395–1409.
20. Gilbert CJ, Lippmann JM, Ritchie RO (1998) Fatigue of a Zr-Ti-Cu-Ni-Be bulk amorphous metal: Stress/life and crack-growth behavior. *Scr Mater* 38:537–542.
21. Menzel BC, Dauskardt RH (2006) Stress-life fatigue behavior of a Zr-based bulk metallic glass. *Acta Mater* 54:935–943.
22. Menzel BC, Dauskardt RH (2008) Fatigue damage initiation and growth from artificial defects in Zr-based metallic glass. *Acta Mater* 56:2955–2965.
23. Hays CC, Kim CP, Johnson WL (2000) Microstructure controlled shear band pattern formation and enhanced plasticity of bulk metallic glasses containing in situ formed ductile phase dendrite dispersions. *Phys Rev Lett* 84:2901–2904.
24. Kuhn U, Eckert J, Mattern N, Schultz L (2002) ZrNbCuNiAl bulk metallic glass matrix composites containing dendritic bcc phase precipitates. *Appl Phys Lett* 80:2478–2480.
25. Ma H, Xu J, Ma E (2003) Mg-based bulk metallic glass composites with plasticity and high strength. *Appl Phys Lett* 83:2793–2795.
26. Hofmann DC, et al. (2008) Designing metallic glass matrix composites with high toughness and tensile ductility. *Nature* 451:1085-U1083.
27. Qiao DC, Fan GJ, Liaw PK, Choo H (2007) Fatigue behaviors of the $Cu_{47.5}Zr_{47.5}Al_5$ bulk-metallic glass (BMG) and $Cu_{47.5}Zr_{38}Hf_{9.5}Al_5$ BMG composite. *Int J Fatigue* 29:2149–2154.
28. Flores KM, Johnson WL, Dauskardt RH (2003) Fracture and fatigue behavior of a Zr-Ti-Nb ductile phase reinforced bulk metallic glass matrix composite. *Scr Mater* 49:1181–1187.
29. Wang GY, et al. (2006) Comparison of fatigue behavior of a bulk metallic glass and its composite. *Intermetallics* 14:1091–1097.
30. Lee SY, et al. (2007) Pseudo-binary phase diagram for Zr-based in situ β phase composites. *J Mater Res* 22:538–543.

31. Brown WF (1989) *Aerospace Structural Metals Handbook* (Metals and Ceramics Information Center, Syracuse, NY), pp 1–30.
32. Rao KTV, Ritchie RO (1992) Fatigue of aluminum lithium alloys. *Int Mater Rev* 37:153–185.
33. Fujita K, et al. (2006) Fatigue strength in nanocrystalline Ti- and Cu-based bulk metallic glasses. *J Jpn Inst Met* 70:816–823.
34. Fujita K, et al. (2008) Ultrahigh fatigue strength in Ti-based bulk metallic glass. *Rev Adv Mater Sci* 18:137–139.
35. He MY, Hutchinson JW (1989) Crack deflection at an interface between dissimilar elastic-materials. *Int J Solids Struct* 25:1053–1067.
36. Harmon JS, Demetriou MD, Johnson WL, Samwer K (2007) Anelastic to plastic transition in metallic glass-forming liquids. *Phys Rev Lett* 99:4.
37. Johnson WL, et al. (2007) Rheology and ultrasonic properties of metallic glass-forming liquids: A potential energy landscape perspective. *MRS Bull* 32:644–650.
38. Lankford J (1985) The influence of microstructure on the growth of small fatigue cracks. *Fatigue Fract Eng Mater Struct* 8:161–175.
39. Miller KJ (1987) The behavior of short fatigue cracks and their initiation. 2. A general summary. *Fatigue Fract Eng Mater Struct* 10:93–113.
40. Tada H, Paris PC, Irwin GR (1985) *The Stress Analysis of Cracks Handbook* (Paris Production, St. Louis).
41. Lee ML, Li Y, Schuh CA (2004) Effect of a controlled volume fraction of dendritic phases on tensile and compressive ductility in La-based metallic glass. *Acta Mater* 52:4121–4131.
42. Fu XL, Li Y, Schuh CA (2007) Homogeneous flow of bulk metallic glass composites with a high volume fraction of reinforcement. *J Mater Res* 22:1564–1573.
43. Peter WH, et al. (2002) Fatigue behavior of $Zr_{52.5}Al_{10}Ti_5Cu_{17.9}Ni_{14.6}$ bulk metallic glass. *Intermetallics* 10:1125–1129.
44. Wang GY, et al. (2005) Fatigue behavior of Zr-Ti-Ni-Cu-Be bulk-metallic glasses. *Intermetallics* 13:429–435.
45. Wang GY, et al. (2008) Fatigue behavior of Zr-based bulk-metallic glasses. *Mater Sci Eng A* 494:314–323.
46. Schuh CA, Hufnagel TC, Ramamurty U (2007) Overview No. 144: Mechanical behavior of amorphous alloys. *Acta Mater* 55:4067–4109.
47. Launey ME, Busch R, Kruzic JJ (2006) Influence of structural relaxation on the fatigue behavior of a $Zr_{41.25}Ti_{13.75}Ni_{10}Cu_{12.5}Be_{22.5}$ bulk amorphous alloy. *Scr Mater* 54:483–487.
48. Menzel BC, Dauskardt RH (2006) The fatigue endurance limit of a Zr-based bulk metallic glass. *Scr Mater* 55:601–604.
49. Dundurs J (1969) Edge-bonded dissimilar orthogonal elastic wedges. *J Appl Mech* 35:650–652.